Journal of
Applied Remote Sensing

RemoteSensing.SPIEDigitalLibrary.org

Method of flight planning for airborne LiDAR using genetic algorithms

Ajay Dashora
Bharat Lohani
Kalyanmoy Deb

SPIE.

Method of flight planning for airborne LiDAR using genetic algorithms

Ajay Dashora,[a,*] Bharat Lohani,[b] and Kalyanmoy Deb[c]

[a]Institute of Infrastructure, Technology, Research and Management, Ahmedabad 380008, India
[b]Indian Institute of Technology Kanpur, Department of Civil Engineering, Kanpur 208016, India
[c]Michigan State University, Department of Electrical & Computer Engineering, Michigan 48824, United States

Abstract. Conventional methods of flight planning for airborne LiDAR are heuristic in nature and use an iterative trial and error approach. A new system-based approach of flight planning is presented in this paper. The presented approach automatically derives flight planning parameters by minimizing the cost of data acquisition, which is represented by flight duration. The flight duration, which is the sum of the strip time and turning time, is minimized using genetic algorithms under the constraints of mapping requirements, hardware limitations, user-defined preferences, and various other requirements. The proposed approach is first validated for conventionally known test cases of regular shapes (rectangular and triangular). Thereafter, it is implemented for an arbitrarily shaped simulated test site with two commercially available airborne LiDAR sensors. Statistical results are presented for the above. Further, flight planning is performed for two real test sites. The demonstrated approach not only produces optimal results, but also avoids the assumptions of conventional methods. Furthermore, the approach requires the least amount of human intervention and, thus, eliminates the subjectivity that is imposed by individual flight planners for determining the flight planning parameters. Encouraged by these results, the authors suggest that the proposed approach can be further developed to include all possible components of flight planning in a future work. © *2014 Society of Photo-Optical Instrumentation Engineers (SPIE)* [DOI: 10.1117/1.JRS.8.083576]

Keywords: flight planning; flight duration minimization; consecutive turning; constrained optimization; genetic algorithms.

Paper 14045 received Jan. 20, 2014; revised manuscript received Jun. 25, 2014; accepted for publication Jun. 26, 2014; published online Aug. 5, 2014.

1 Introduction

Airborne LiDAR data are proving their utility in many areas of general and specific interest, like airport surveys, engineering and construction, forestry, oil and gas exploration, mining, transportation (highway or corridor surveys), utility surveillance and monitoring, water management, coastal zone monitoring, telecommunications, noise modeling, three-dimensional visualization, etc.[1–4] For all applications, the cost of LiDAR data depends upon several factors. One of the major cost elements is the cost of flying. Unarguably, reflying due to mission failure is an unaffordable option. Consequently, a successful flight mission heavily depends on a successful flight plan.[5]

A flight planning exercise attempts to derive flight planning parameters by considering various components such as sensors, user requirements, mapping standards, the aerial platform, and field limitations. Theoretically, the flight planning exercise should achieve the required characteristics of the LiDAR data with a minimum cost.

Conventionally, a flight planning exercise is performed either by a manual approach or a semiautomatic approach. The manual approach utilizes nomograms (or graphs) and performs all calculations manually.[6,7] However, the semiautomatic approach employs software tools,

*Address all correspondence to: Ajay Dashora, ajay.dashora@iitram.ac.in; ajaydashora@gmail.com

e.g., Topoflight, ALTM-NAV, ASCOT, IGI Plan, etc. These tools work through an iterative trial and error process, where a user starts with an initial estimate of the flight planning parameters and, thus, is expected to use his experience for successful flight planning. In either of the conventional approaches, turning time (TT) is not explicitly modeled, but assumed to be constant.[8] Furthermore, private communications with Dr. Adriaan Combrink of C K Aerial Surveys (South Africa), who frequently conducts the flights for airborne LiDAR data acquisition in the African continent, reveals that even after flight planning with the available commercial tools, a manual intervention for better decision making is required.[9] Consequently, the subjectivity in decision making for flight planning by individual flight planners cannot be avoided.

On the other hand, according to a paper published by Saylam[5] in 2009, the flight planning aspect of airborne LiDAR is not ever discussed in detail by researchers. Recently, a research study by Tian et al.[10] discusses the features and limitations of the above-mentioned commercial and available research tools for airborne LiDAR flight planning. Also, the authors compare these tools and further indicate that none of these includes the parameter optimization aspect for minimization of flight duration (FD). Tian et al.[10] further presented a simulation-based study for a flat rectangular area of interest (AOI) without considering the TT (or switching time) between flight lines. Assumptions made by Tian et al.,[10] like prefixing various parameters, the decision to fly along the longer side of the AOI, and deciding *a priori* spot spacing for achieving uniformity, led to the loss of desired flexibility and philosophy for designing and planning the survey. Moreover, deciding the point repetition frequency (PRF) according to the flying height for differentiating two pulses emitted in sequence is redundant in practice as scanner specifications are prepared after calibration. Therefore, the derived parameters are purely of theoretical significance. As a result, the demonstrated simulation study by these authors does not depict the real-world physical system of airborne LiDAR data acquisition, yet it successfully highlights the limitations of current approaches of flight planning for airborne LiDAR. On the other hand, Dashora et al.[11] discuss the optimization aspects of the flight planning problem for airborne LiDAR and present a two-step procedure with a rigorous mathematical treatment of the problem.

In view of the above discussion, this paper presents a new methodology for flight planning, which considers the entire flight planning as a single system and minimizes the FD while also satisfying the data requirements. This paper is organized into six sections. An introduction, state-of-the-art practices, and the available literature on flight planning are presented in Sec. 1. Before developing the mathematical description of the problem in Sec. 2, the minimum prerequisites of a flight planning exercise, which include inputs, assumptions, user requirements, and information about the airborne LiDAR scanner models, are mentioned. The paper then develops a mathematical definition of the objective function for FD and constraints considering the LiDAR sensor hardware and the user requirements in the same section. In Sec. 3, an optimization scheme that minimizes the FD (or objective function) under the constraints is presented. In the next section, the proposed approach of flight planning is first validated for well-known test cases, e.g., long strip and triangular AOI. Then, the statistical experiments are conducted for the flight planning for an arbitrary-shaped AOI with two distinct LiDAR sensors, which are mentioned in Sec. 3. The developed approach is implemented for two real test sites in Sec. 4. The results are presented and discussed with statistical analysis in Sec. 5. Conclusions along with possible future work are presented in Sec. 6.

In this paper, the definitions of fundamental terms (viz., half scanning angle ϕ, scanning frequency f, flying height H, flying speed V, PRF F) and the derived terms [viz., effective swath B, data density ρ, along-track spacing D_A, across-track spacing D_S, nominal pulse spacing (NPS)] for airborne LiDAR scanning are adopted from Baltsavias[12] and Wehr and Lohr.[13]

2 Conceptualization of Flight Duration

2.1 *Assumptions*

This paper assumes a horizontal and flat terrain. Further, it is assumed that appropriate time windows for a global positioning system (GPS) are available. The weather is calm and, thus, the wind speed is ignored.

2.2 *Area of Interest, User Requirements, and LiDAR Sensors*

The AOI, which is a closed polygon and may be irregular in shape, is the basic input and prerequisite information. The map coordinates of the AOI (x, y) in a reference frame are available.

Among the user requirements, data density and spatial uniformity of the LiDAR data are considered. Consequently, the data density or NPS, which may be required in the range of $0.25\ \text{points}/\text{m}^2$ (1 point in $4\ \text{m}^2$) to $60\ \text{points}/\text{m}^2$,[14,15] is supplied by the user. Further, as recommended by Heidemann,[16] for all scanning patterns, the minimum strip overlap and uniform spacing in along-track and across-track directions (for ensuring spatial uniformity and avoiding clustering in the data) are also taken into account.

The LiDAR sensors, Optech's ALTM 3100EA and Leica's ALS50-II, which create bidirectional Z-shaped scanning patterns, are used. Relevant characteristics and features of sensors, which are available in online specifications or obtained from manufacturers, and their critical role in flight planning are discussed in Sec. 3. Section. 3.1 present the mathematical formulations for objective function and constraints, which are adopted from Refs. 8, 11, and 17.

2.3 *Formulation of Flight Duration*

LiDAR data are collected by flying an aircraft, equipped with sensors, over straight and parallel flight lines, thus covering the parallel strips on the ground (as shown in Fig. 1). In a certain flying direction (θ), the length of flight line is considered from one end of the AOI to the next end and the width is determined by the swath, which maintains a sufficient lateral overlap with the neighboring strip. At the end of each flight line, an aircraft negotiates a turn to reach the adjacent flight line. For a given AOI, an aircraft covers it by travelling over a finite number of flight lines. Thus, the total time of flight or FD consists of the time required for flying over the strips [strip time (ST)] and the time required to negotiate the turns [turning time (TT)].

For a given direction of flying (θ) with respect to the x axis of the map coordinate system as shown in Fig. 1, a new flight line coordinate system can be considered, where the X axis is along the flight direction. The rotated coordinates of the AOI are obtained by conformal transformation as[18]

$$\begin{bmatrix} X \\ Y \end{bmatrix} = \begin{bmatrix} \cos\theta & \sin\theta \\ -\sin\theta & \cos\theta \end{bmatrix} \begin{bmatrix} x \\ y \end{bmatrix}. \tag{1}$$

The extent of the AOI along the the Y axis (or height of the AOI) in the flight line coordinate system is equal to the difference of the maximum and minimum Y coordinates in the AOI.

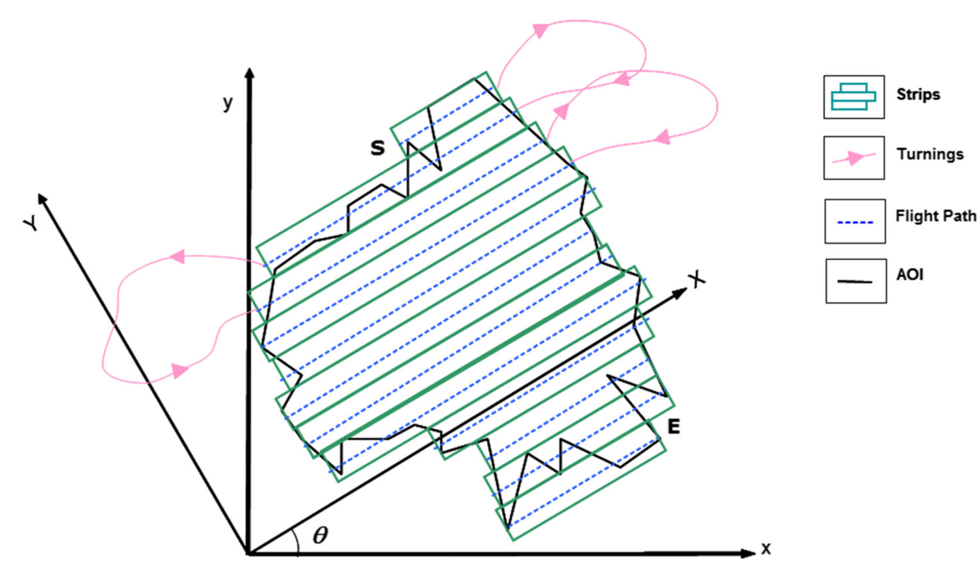

Fig. 1 Schematic view of area of interest (AOI), flight strips, flight lines, and turns.[16]

Similarly, the length of a strip is equal to the extent of the AOI in the X axis direction (Fig. 1), which will be different for different strips depending upon the location of the strip along the Y axis. The minimum (and integer) number of flight lines are calculated by dividing the height of the AOI by the effective swath (B) and rounding the real number to higher side thus calculated as

$$n = \text{ceiling}\left(\frac{Y_{\max} - Y_{\min}}{B}\right). \tag{2}$$

Here, the effective swath, which is equal to the swath minus the overlap, is equal to the separation between flight lines. For an overlap fraction of η, a half scan angle of ϕ, and a flying height of H above datum, the effective swath (B) is written as

$$B = (1 - \eta)(2\ H \tan\ \phi). \tag{3}$$

For n number of flight lines calculated by Eq. (2), there will be $n - 1$ number of turns. Since, FD is the total time duration required by an aircraft to cover the strip and turns with constant speed (V), FD (T) can be formulated as

$$T = \frac{\sum_{i=1}^{n} L_i}{V} + T_t. \tag{4}$$

In Eq. (4), L_i represents the length of the i'th flight strip (flight path on the i'th flight line on the ground or the center line of the i'th strip on the ground) and T_t is the time required for $n - 1$ turns. The length and location of the flight line of the i'th strip for given θ will depend on the size of the effective swath (B) as it affects the number of strips [Eq. (2)]. As indicated earlier, according to the current practices in the field, the TT between the two adjacent flight lines is considered constant. Contrarily, as the length and location of the adjacent flight lines affect the TT, this paper proposes to model it for a better estimate for optimization.

Turning between the flight lines can be performed by consecutive, nonconsecutive, and hybrid turning mechanisms.[8] Also, Dashora and Lohani[8] describe the modeling of various turning mechanisms and calculations of the TT. In order to demonstrate the new method of flight planning in this paper, a consecutive turning mechanism is adopted from Dashora and Lohani[8] with some simplifications. In the forthcoming discussion, the consecutive turning mechanism, with the assumptions adopted in this paper, is briefly explained and the desired formulations are presented.

2.3.1 *Turning time for consecutive turning mechanism*

There are two possibilities for turning onto a consecutive flight line: the effective swath (B) is less than the space required for the width of the turn (h_t) and vice versa.[8] For the former case, the schematic view of a consecutive turn between two adjacent flight lines is shown in Fig. 2. The flight path on the turn is shown by the firm black line.

An aircraft exits a flight line from point A and reaches to point C so as to form a half circular turn of width h_t to approach the right end of the next flight line. However, instead of the right end of the next flight line, it is preferable to reach point E, which is situated at a distance equivalent to the cushion length (Vt_C) from the right end of the next flight line. The symbol t_C represents the cushion period, which provides sufficient time for a pilot to align the aircraft correctly on the flight line before it reaches the starting point of the next flight line.[8] The resulting cushion length, except for the first flight line, modifies the coordinates of the left and right ends of the alternative flight lines, e.g., the right end of the second flight line and the left end of the third flight line, and so on.

As shown in Fig. 2, the trajectories from point A to C and further from C to D consist of circular curves that meet straights. Therefore, an aircraft would need to navigate from a straight line to a circular curve and again back to a straight line. This is possible using transition curves, which connect the straight line trajectory to the circular trajectory and vice versa. Transition curves occur at point A, between points A and C, point C, and point D.[8] In this study, the calculations of time durations related to transition curves are ignored for simplicity. Consequently,

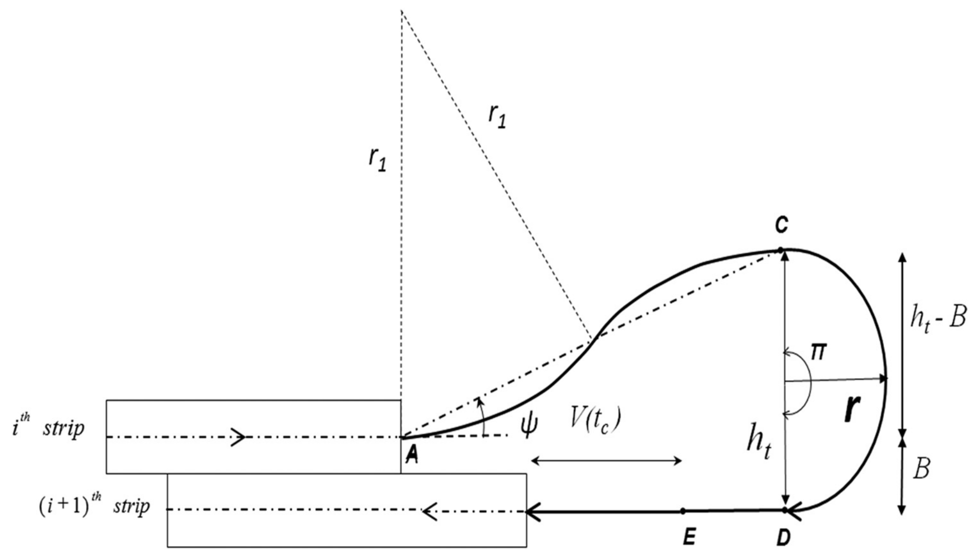

Fig. 2 Schematic view of two consecutive flight lines and flight path with cushion period in a consecutive turn.[8]

the width of the circular turn (h_t) in Fig. 2 is equal to twice the radius of the circular turn (r), which is given by[19]

$$r = \left(\frac{V^2}{g \tan \beta_m}\right). \tag{5}$$

In Eq. (5), β_m represents the maximum banking angle. For feasible turning between points A and C, the maximum value of the change in the heading angle ψ is given by[8]

$$\psi_{\text{Max}} \le \sin^{-1}\left[\sqrt{\left(\frac{h_t - B}{8V}\right)\dot{\psi}_{\text{Max}}}\right]. \tag{6}$$

It should be noted that in all equations, wherever h_t appears, $h_t = 2r$.

In Eq. (6), $\dot{\psi}_{Max}$ is the maximum allowable rate of turning for the heading angle, which is restricted to the standard rate of turning (3 deg per second). On the other hand, when the required angle ψ (heading change) is less than ψ_{Max}, the rate of turning $\dot{\psi}$ is calculated by modifying Eq. (6) as[8]

$$\dot{\psi} = \left(\frac{8V \sin^2 \psi}{h_t - B}\right). \tag{7}$$

The radius of turn (r_1) for each of the two circular curves lying between points A and C is calculated as[8]

$$r_1 = \left(\frac{V}{\dot{\psi}}\right). \tag{8}$$

Therefore, for a pair of consecutive flight lines, the distance from A to D via C is given by

$$L' = 4r_1 \sin^{-1}\left(\frac{L_1}{4r_1}\right) + \pi r + \Delta X + V t_C; (\text{if } B < h_t). \tag{9}$$

In Eq. (9), the distance L_1 is the available length of the straight line AC between points A and C, which is given by[8]

$$L_1 = \left(\frac{h_t - B}{\sin \psi}\right). \tag{10}$$

Also, in Eq. (9), ΔX symbolically represents the difference of the X coordinate of the end of the upper flight line and the modified X coordinate of the lower flight line. This difference of X coordinates is equal to the distance between D and E in Fig. 2. Further, the cushion length (Vt_C) in Eq. (9) represents the extra travel length due to the modification of the X coordinate of the lower flight line.

On the other hand, when the effective swath (B) is more than or equal to the required width of the turn ($2r$), the aircraft will turn without changing the heading angle (i.e., $\psi = 0$). In this case, in addition to the two quarters of a circular turn, the interspread with a straight length ($B - 2r$), the difference between the X coordinates of the ends of the flight lines (ΔX), and the distance equivalent to the cushion period (Vt_C) should be added. Therefore, the total distance during a turn from the end of a flight line to the end of the consecutive flight line is given by

$$L' = \pi r + (B - h_t) + \Delta X + Vt_C; (\text{if } B \geq h_t). \tag{11}$$

It is evident from the above discussion that it is possible to determine the numerically feasible values of FD using Eqs. (4) to (11). However, the FD is also constrained by the user requirements and standards. The following Sec. 2.4 discusses the fundamental constraints on the FD imposed by the mapping standards[16] and the user requirements.

2.4 *Constraints on Flight Duration*

As mentioned earlier, a user demands a minimum data density (e.g., 10 points/m^2). The general expression of data density, independent of the type of scanning pattern, shows the number of points captured in the unit area in 1 s as[12]

$$\rho = \frac{F}{(2\,H \tan \phi)V}. \tag{12}$$

However, numerically and in real practice, it is not possible to achieve a fixed value of data density. Therefore, a range can be specified using some user-specified tolerance. According to Saylam,[5] 10 to 50% tolerance on the higher side in data density can be considered. Therefore, considering a 10% positive tolerance in the targeted data density of 10 points/m^2 will result in a 10 to 11 points/m^2 range of data density.

Apart from that, for uniformity in the spatial distribution of LiDAR data, there should be a relationship between across-track and along-track spacings. Figure 3 is an exaggerated view of the Z-shaped scanning mechanism where the across-track spacing between two successive points in a scan line is not uniform and is minimum at the center and maximum at the ends.

For uniform spatial distribution of LiDAR data, the across-track (D_S) and along-track (D_A) spacings should be comparable. Therefore, the difference of the average across-track spacing and the average along-track spacing for a Z-shaped scan line pattern is constrained by a threshold (ε_S). The resulting mathematical expression is expressed as

$$|D_A - D_S| = \left|\left(\frac{V}{f}\right) - \left(\frac{2fB}{F}\right)\right| \leq \varepsilon_S. \tag{13}$$

Equations (12) and (13) ensure the minimum data density and maximum average spacing in longitudinal and lateral directions for both sensors. Minimizing the FD [Eq. (4)] under the constraints imposed by Eqs. (12) and (13) is a single objective, multivariable, multiconstraint optimization problem.

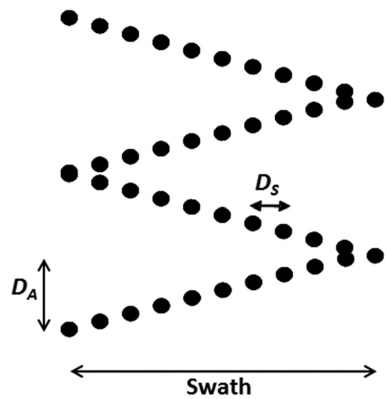

Fig. 3 Z-shaped or bidirectional scanning pattern.

3 Constrained Optimization of Flight Duration

Equations (1) to (13) contain the flying direction (θ), scanning angle (ϕ), scanning frequency (f), flying height (H), aircraft speed (V), and PRF (F) as six unknown variables that are to be determined by minimizing the FD under the constraints. Among the six variables, the scanning frequency, scanning angle, and PRF are the parameters of the scanner hardware. However, the aircraft speed, flying height, and flying direction are the flight parameters. Also, FD is the time in the air required for capturing data and does not include the duration for takeoff, landing, trial runs, or dry runs.

3.1 *Test Area of Interest and LiDAR Sensors*

As flight planning is performed before data acquisition in the field, a simulated test site with real-world conditions is also appropriate for the flight planning exercise. Therefore, an AOI in the form of an arbitrary area is scanned and digitized. This resulted in an AOI polygon with 1012 vertices having a total area of size 4.08 km^2 (as shown in Fig. 4), which is likely the extent of a small residential or industrial unit.

Among the six variables of input vector or design vector, the scanner parameters are discrete and the flying parameters are continuous. All characteristics (working range and least count) of ALTM 3100EA and ALS50-II, and the flying parameters relevant to this study are shown in Tables 1 and 2. The functional range of the scanner parameters are taken from the specifications of ALTM 3100EA[20] and ALS50-II.[21] The working range of the aircraft speed and the least counts of scanning frequency and scanning angle were obtained by private communications

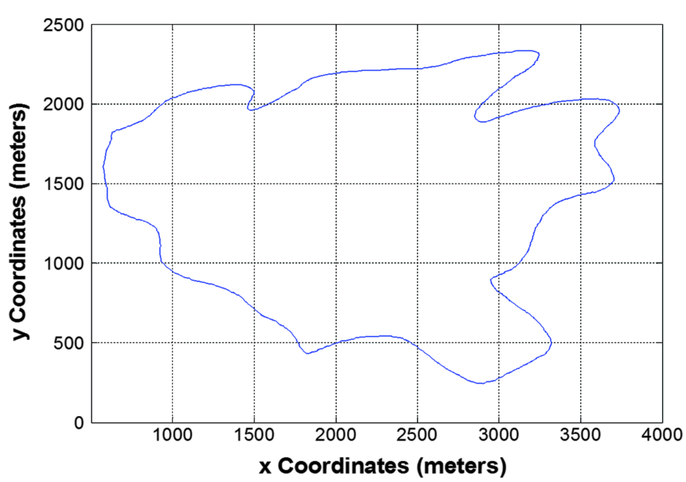

Fig. 4 Schematic view of AOI.

Table 1 Details of scanning and flying parameters for Optech's ALTM 3100EA sensor.

Parameters	Range	Least count
Flying height (H)	305 to 3500 m	Continuous
Flying direction (θ)	0 to 360 deg	Continuous
Aircraft speed (V)	45 to 72 m/s	Continuous
Scanning frequency (f)	1 to 70 Hz	1 Hz
Scanning angle (ϕ)	1 to 25 deg	1 deg
PRF (F)	33 kHz (if $0 \le H \le 3500$ m) 50 kHz (if $0 \le H \le 2500$ m) 70 kHz (if $0 \le H \le 1700$ m) 100 kHz (if $0 \le H \le 1100$ m)	

Note: PRF, point repetition frequency.

Table 2 Details of scanning and flying parameters for Leica's ALS50-II sensor.

Parameters	Range	Least count
Maximum distance or slant range (r)	305 to 7563 m	Continuous
Flying direction (θ)	0 to 360 deg	Continuous
Aircraft speed (V)	45 to 72 m/s	Continuous
Scanning frequency (f)	1 to 90 Hz	0 to 1 Hz
Field of view (FOV)	1 to 75 deg	1 deg
PRF (F)	20 to 160 kHz	100 Hz

with Mariusz Boba of Optech Inc. (Canada) and Jake Carroll of Bearing Tree Land Surveying L.L.C. (USA).[22,23]

In addition to this, due to the physical mechanism of scanning, the ALTM 3100EA sensor also imposes a constraint. This constraint is called the scanning product and is expressed as[20]

$$f\phi \le 1000. \tag{14}$$

Similarly, for Leica's ALS50-II, the scanning frequency and PRF are constrained by the maximum scanning frequency ($f_{\max}$) and maximum PRF ($F_{\max}$), respectively. The maximum scanning frequency as a function of FOV (or 2ϕ) is provided as[21]

$$\begin{aligned} f_{\max} = {} & 8068.7995 \times 10^{-12}(\mathrm{FOV}^6) - 2321.956 \times 10^{-9}(\mathrm{FOV}^5) \\ & + 271.32545 \times 10^{-6}(\mathrm{FOV}^4) - 16.673046 \times 10^{-3}(\mathrm{FOV}^3) \\ & + 0.58391112(\mathrm{FOV}^2) - 11.956674(\mathrm{FOV}) + 166.2779. \end{aligned} \tag{15}$$

The PRF for the Leica sensor can be varied at the rate of 100 Hz. The maximum value of the PRF ($F_{\max}$) is also provided in the form of a curve as a function of the slant range (r).[21] In order to calculate the value of the maximum PRF for the selected value of slant range, the given curve is digitized and intermittent values of the maximum PRF are calculated by linear interpolation. The reason for using linear interpolation is that fitting higher-order polynomials is found to produce erroneous results.

3.2 *Flight Duration Minimization by Genetic Algorithms*

Equation (4) represents the FD as a single-objective function to be minimized under the constraints. Due to turning between the parallel flight lines of different lengths, the objective function becomes a nonlinear and discontinuous mathematical function. Moreover, it may also show multimodal behavior. Furthermore, the objective function and constraints are functions of discrete and continuous variables, which cannot be separated. Additionally, initial guesses of the parameters are not available. Therefore, conventional or classical optimization methods, which are sensitive to the initial estimates of the parameters and may demand continuity of the objective function, are not applicable. Consequently, the genetic algorithms (GA) are utilized for minimization of the objective function in the present case.

Unlike the conventional optimization methods, GA are statistical methods independent of any assumptions of the objective function (unimodality, continuity, existence of derivatives, etc). The search procedure starts with a randomly generated multiple set of input vectors (or population of design vectors) in the given ranges of parameters and an objective function is calculated for each design vector. The calculated objective function (also called the fitness function) information is further utilized to generate the next population of input vectors through three genetic operators, namely, selection, cross over, and mutation. In the case of a minimization problem, to form the next generation of the population, the fitness function of less value is considered as having more weight.[24]

In the context of flight planning for airborne LiDAR, a working principle of the generic GA and derivation of the flight planning parameters are demonstrated pictorially in Figs. 5 and 6.

Figure 5 displays the generic process of GA for the flight planning system. With user input (ranges of parameters, AOI, data requirements, etc.), samples or a population of parameters are created as combinations of random values of parameters in their prescribed ranges. For this first set of samples (or population) of parameters, the values of the FD and constraints are calculated. This information (samples with corresponding FD and constraint values) is then passed to the mating pool. The mating pool regenerates a set of new samples (or new population) using selection, cross over, and mutation, which are explained later. This process of regeneration is repeated for a specific number of iterations, which are called generations. Once the prescribed number of generations are completed, the GA provide values of the best sample in the last generation as parameters.

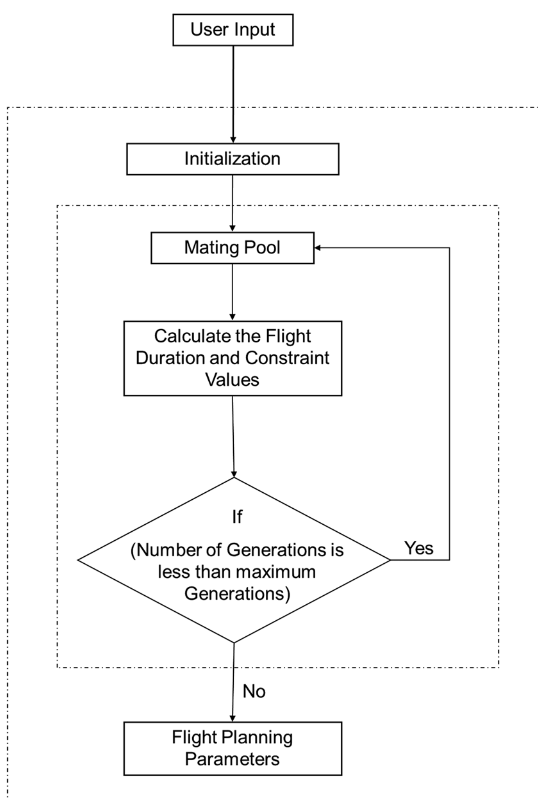

Fig. 5 Process of determining flight planning parameters by genetic algorithms (GA).

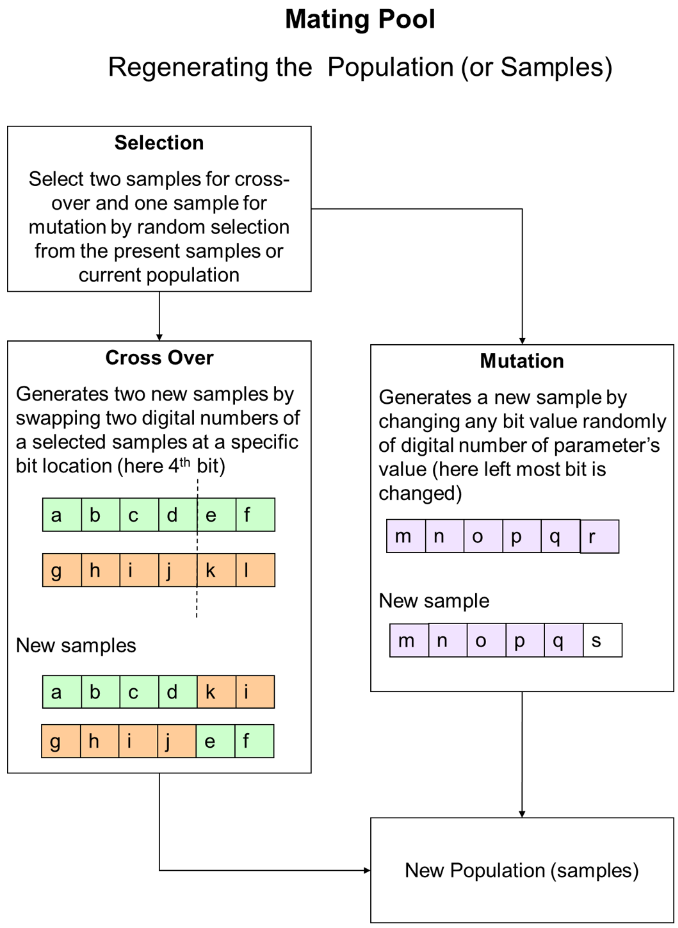

Fig. 6 Generation of new population from old population by GA using selection, cross over, and mutation in mating pool.

An ideal GA ensures that the regeneration process in the mating pool refines the parameter values of the samples in such a manner that the FD and constraint violations are minimized continuously over generations. Figure 6 demonstrates the process of regeneration of a new population from an old population in the mating pool.

For the given population of any generation, the mating pool assigns rank (or weight) to each individual sample according to its FD and constraint values. For minimizing the FD under the constraints, a sample having less FD and less constraint violations receives a higher rank and is preferred to participate in the regeneration process. The mating pool randomly selects two samples and generates two new samples using a cross-over operator. Figure 6 depicts the cross-over of two values of a parameter, which are shown schematically as digital numbers by alphabets. According to the figure, the cross-over performs the swapping of these digital numbers and creates two new numbers. As a consequence, the quality of the new samples (new population), which is generated by cross-over, depends upon the quality of the available samples (current population). Therefore, bias in the information carried by the samples is expected to get transferred by cross-over from the current population to the new population. As a result, as stated earlier, cross-over might lead to a state where there is no improvement in the fitness values (FD in this case) of the newly generated samples. This bias is alleviated by mutation, which randomly selects a sample and occasionally changes its value. In Fig. 6, mutation changes the digital value of a sample by altering the value at the location of the least significant bit. Locations of cross-over or mutation may be predefined or may be chosen randomly. Moreover, the number of samples to be regenerated by cross-over or mutation is also predefined. In this way, new population is supplied by the current population using cross-over and mutation genetic operators in GA. For further details on GA, interested readers may refer a book on GA by Goldberg.[24] Section 3.3 implements the optimization scheme for the flight planning system.

3.3 *Numerical Implementation of Optimization Scheme*

The aforementioned optimization scheme is implemented in C language. As explained earlier by Fig. 2, flight strips (and flight lines) are separated by the distance of the effective swath (B). In order to determine the coordinates of the strips and the flight lines, the coordinates of the vertices of the AOI (x,y) are rotated by flying direction (θ). After rotation, the intersection points of the upper and lower edges of the flight strips with the AOI boundary are calculated and the maximum of these are taken as the coordinates of the ends of the flight strip. The coordinates of the ends of a center line (or flight line) of a strip are used for the calculations of both the TT and ST.

A real coded genetic algorithms (RGA) code, which is developed and made available online by Kanpur Genetic Algorithm Laboratory, is used for performing optimization. All details pertaining to reproduction, mutation, cross-over and constraint handling strategies are documented in the available code. The RGA code can generate both continuous and discrete parameters using random numbers. Integer (discrete) parameters (like scanning frequency and half scan angle) are generated in two ways: first by the binary string of a specific bit, where half scan angle values in the range from 1 to 25 can be created by converting a 5-bit binary number to a decimal number. On the other hand, according to the second method, the values of parameters (say ϕ) can also be generated by a round-off function on randomly generated real values of a variable (say ϕ_R) and its least counts (ϕ_L) as

$$\phi = \mathrm{round}\left(\frac{\phi_R}{\phi_L}\right)\phi_L. \tag{16}$$

The functional ranges of the values of the parameters are specified in Tables 1 and 2. The flying parameters are modeled as continuous variables within the given ranges. Practically, considering the minimum flying altitude of 200 m for eye safe criterion and 305 m (1000 feet) for minimum allowable flying altitude in India,[25] the lower range of the flying height comes to 305 m. The maximum range of the flying height is taken as the maximum flying height of the sensor. The PRF is calculated according to the flying height value using a random variable for Optech's ALTM 3100EA sensor. However, for Leica's ALS50-II sensor, it should be noted that the PRF is a direct function of the slant range (not the flying height) and it measures the discrete values of the field of view (FOV) (not the half scan angle). Therefore, for the ALAS50-II sensor, instead of the flying height and half scan angle, the slant range and FOV, which are, respectively, continuous and discrete variables, participate in the optimization process as the parameters. Consequently, the flying height and half scan angle are first calculated as the derived variables, respectively, from the slant range and FOV and then used for the calculation of the swath, effective swath, FD, and other variables.

The discussed approach of constrained minimization of the FD is first validated for the known test cases and then implemented for the simulated AOI. In the case of simulated AOI, as the nature of the problem is unknown, optimization is performed for varying the number of population counts, viz., 60, 120, 200, 300, 400, and 500, with 200 generations for each case. Cross-over and mutation probabilities of 0.8 and 0.125 are used for both discrete and continuous parameters. Validation and results for simulated AOI are presented in Sec. 4.

4 Results and Validation for Simulated AOIs

The developed approach is tested and validated for conventionally known and intuitively obvious flying directions (i.e., longest direction) for rectangular and triangular AOIs. In these experiments, for validating the approach, the effects of the cushion period and TT are highlighted.

4.1 *Intuitive Validation*

Simulation experiments are designed for intuitive cases of long rectangular strips and triangular areas with different combinations of TT and cushion period. Data density in the range of 10 to 11 points/m^2 and an absolute difference of spacings of 0.1 m ($\varepsilon_S = 0.1$ m) are considered. The following results, which are intuitive in nature, are obtained.

A horizontal long and narrow strip (10 km long and 50 m wide), which has an intuitive, theoretical, and obvious direction of flying, i.e., along its length, is solved using the developed optimization scheme with and without the time of turnings' options for the ALTM 3100 EA sensor. It should be noted that the narrow width of the strip (50 m) is deliberately selected to form a single flight line. For optimization with a constant time of turning (3 min), a GA with 200 generations and a population size of 200 successfully determine all six flight planning parameters automatically. Moreover, the flying direction is determined along the length of the strip. On the other hand, without considering the TT, the GA suggest the flying direction along the shorter direction of the long strip. Interestingly, due to zero value of the TT, flying along the shorter direction divides the long strip in multiple flight lines and still gives a smaller value for the FD. It shows that considering only the strip time and ignoring the TT leads to an incorrect flying direction.

In the second experiment, the effect of the cushion period on the TT is analyzed. A horizontal triangular area with a 10-km-wide base and a 5-km length, which are aligned in the y and x directions, respectively (as shown in Fig. 5), is selected as the AOI. In the first case for this AOI, the cushion period was considered to be zero. As the lengths of the strips are decreasing from the base to the vertex of the AOI in the x direction, it is intuitive to travel in a direction across which the strip size increases from shorter to longer lengths. The GA detected the negative Northing direction (270 deg or −ve y axis) as the flying direction (from vertex to base).

Contrary to the above case with a zero cushion period, when the cushion period is taken as 30-s, the GA detected a positive Northing (90 deg or +ve y axis) as the flying direction. The cushion period of 30-s with a speed of 50 m/s is equivalent to a 1500 m increase in the length of a strip that is to be approached by an aircraft (as shown in Fig. 7). As a consequence, with a 30-s cushion period, it is economical to travel in the opposite direction as that of the flying direction without a cushion period, i.e., travel from the base to the vertex or the positive Northing direction (90 deg or +ve y axis).

The above experiments with the rectangular and triangular AOIs, with and without a cushion period, present some important inferences about the TT. First, as in real practice where the AOI is of arbitrary shape, the hypothesis of ignoring the TT is certainly inferior to that which assumes it as a constant. Furthermore, for the strips of different lengths in an AOI, the TT for each turn is different and is also influenced by the cushion period, which is decided as per the preferences of the pilot and flying crew. Therefore, simulation experiments suggest that modeling of the TT and its inclusion in the objective function for determining total FD is most warranted as it provides the criterion for the GA for better decision making.

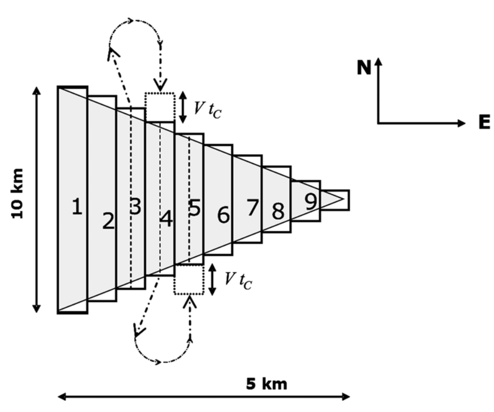

Fig. 7 Schematic view of 10 flight lines with cushion length[16] (figure not to scale).

4.2 *Statistical Results for Test Area*

For the simulated AOI, both the ST and TT are considered in the objective function. The designed data density is 10 to 11 points/m^2. As recommended by Heidemann,[16] the following constraints are adopted:

1. Minimum overlap fraction is 10%.
2. Variation in average across-track and along-track spacing is restricted to 10% (i.e., the ratio of maximum absolute difference of average along-track and across-track spacing to along-track spacing is taken as 10%).
3. In order to avoid sparseness in the LiDAR data at the edges of a swath, the maximum FOV of a LiDAR scanner is limited to 40 deg.

For two LiDAR sensors, with their specified range of flying parameters and scan parameters, flight planning parameters are determined automatically by RGA code. In order to analyze the performance of the RGA code with statistical measures, the code was run 30 times for 200 generations with population counts of 60, 120, 200, 300, 400, and 500. The results are shown in Tables 3 and 4. Statistical ranges of the results are identified manually for a 99% confidence interval. Any result which is out by three times standard deviation (σ) with respect to the mean value on either side, is declared an outlier. However, the success rate of the method is evaluated by only rejecting the outliers on the higher side (>mean + three times standard deviation). Tables 3 and 4 present the results with statistical measures.

Table 3 Flight duration (FD) statistics (seconds) for simulated area of interest (AOI) for ALTM 3100EA sensor.

Population	60	120	200	300	400	500
Minimum (best)	1756.3	1756.2	1754.8	1754.6	1754.6	1754.6
Mean (average)	1922.6	1941.5	1858.4	1918.6	1765.3	1758.6
Std. dev. (1σ)	336.6	333.3	233.6	300.9	15.9	4.5
Mean $+ 3\sigma$	2932.5	2941.5	2559.1	2821.2	1813.2	1772.2
Mean $- 3\sigma$	912.8	941.5	1157.7	1016.0	1717.3	1745.1
No. of runs	30	30	30	30	30	30
No. of outliers	2	2	0	0	2	0
Success rate (%)	93.7	93.7	100	100	93.7	100

Table 4 FD statistics (seconds) for simulated AOI for ALS50-II sensor.

Population	60	120	200	300	400	500
Minimum (best)	1590.3	1588.8	1595.0	1592.8	1590.6	1590.6
Mean (average)	1969.2	1809.3	1771.5	1695.6	1656.2	1643.7
Std. dev. (1σ)	388.7	225.9	187.5	93.1	76.1	68.8
Mean $+ 3\sigma$	3135.4	2487.1	2334.1	1974.8	1884.6	1850.1
Mean $- 3\sigma$	803.0	1131.5	1208.9	1416.4	1427.9	1437.4
No. of runs	30	30	30	30	30	30
No. of outliers	2	1	0	1	2	2
Success rate (%)	93.7	96.7	100	96.7	93.3	93.3

It can be observed from Tables 3 and 4 that an increase in the population count affects the minima determination in the present problem and the same level of minima is observed by all the population counts with almost the same number of outliers. However, higher population counts increase the reliability as the values of average and standard deviation of the solutions are reduced. The success rates above or equal to 90% with all population counts indicate a reasonable level of consistency for the GA. Increasing the population count up to 500 improves the results drastically, however, it does increase the computation time. By increasing the population to 600 and above, for which results are not shown, the standard deviation is further reduced, but the minimum (or best) cannot be improved. On the other hand, due to the random process of population generation, at times more optimistic as well as more pessimistic results are also obtained. For example, with population counts of 120 for the ALS50-II sensor, the best result obtained is better than that with the other population counts. Contrary to that, the number of outliers increased with an increase in the population over 200. Similarly, for the ALTM 3100EA sensor, with a population count of 300, the standard deviation and the number of outliers are unexpectedly higher than that of the lower population counts. This behavior may be due to the discrepancy in random number generation that occasionally happens.

It is also observed that increasing the generations over 200 does not yield better results.

The flight planning parameters, which are obtained as the best results of the simulation experiment for the simulated AOI using Optech's ALTM 3100A (by 300 population count) and Leica's ALS50-II (by 400 population count) are presented in Table 5. For Leica's ALS50-II, the flying height is derived from the range that is used as one of the variables in optimization by the GA.

4.3 *Validation for Flight Planning Parameters*

The results obtained by GA for the simulated AOI are optimal solutions of the constrained FD minimization problem. However, as data density and along- and across-track spacings are average criterions in the optimization process, their actual values should be confirmed using test data. For spatially uniform and cluster-free data, Heidemann[16] mentions that 90% of the area around the center of the swath is to be overlaid with square-sized cells, each having a size of two times the NPS, and 90% of these cells in the grid should be occupied by at least one LiDAR point.

In order to generate the data for validation of the NPS, artificial LiDAR data are generated using the software LIMULATOR,[26] which is an independent data generating utility. The software requires flight planning parameters and precision of the various sensor units [GPS, inertial measurement unit (IMU), etc.] as the input for generating LiDAR data. For validation purposes, 5-cm horizontal and 7.5-cm vertical errors (1σ) are assumed to be contributed by the GPS unit. Errors (1σ) in roll, pitch, and yaw are taken from the specifications of the Applanix PosAV510 IMU unit. The remaining error factors, like bore sight values, beam divergence of the laser pulse (or laser foot print), etc., are ignored for simplicity. With these mentioned error measures,

Table 5 Flight planning parameters for simulated AOI for two sensors.

Parameter	Values	
	ALTM 3100EA	ALS50-II
Flying height (H)	904.824 m	893.303 m
Flying direction (θ)	193.346 deg	188.717 deg
Aircraft speed (V)	45.00 m/s	45.06 m/s
Scanning frequency (f)	70 Hz	70.3 Hz
Half scan angle ($\pm\phi$) or FOV (2ϕ)	± 7 deg	15 deg FOV
PRF (F)	100 kHz	106,500 Hz

LiDAR data are generated by the LIMULATOR by employing the flying parameters obtained by the GA (shown in Table 5) for an area with its width and length equal to the swath ($2H \tan \varphi$) and flying speed (V), respectively. It is found that more than 90% of the cells are occupied by at least one LiDAR point for both sensors.

5 Flight Planning for Real Test Sites

After conducting simulation experiments and successfully validating their performances, the GA based flight planning system is implemented for two real test sites. These sites, namely Big Smith Creek (BSC) and Harry Channel (HC), are situated in the Mackenzie valley of Canada. Coordinates of the vertices of these AOIs and other airborne LiDAR survey requirements can be obtained from online contract information provided by MERX.[27] BSC and HC sites, respectively, occupy 12.48 and 43.21 km^2 areas on the map. Google Earth images of these sites are shown. The BSC site (as shown in Fig. 8) is close to rectangular in shape and has dimensions of 2.6 km by 5.7 km in the orthogonal directions. Contrarily, the HC site (as shown in Fig. 9) is close to being square in shape and shows dimensions of 7.2 km by 6.7 km (the dimension of side that is closer to the lower edge of Fig. 9 is longer and is equal to 7.2 km).

As per the online contract information, it is desired to collect airborne LiDAR data with a minimum of 1.5 $\mathrm{points/m^2}$ data density. For the purpose of this study, these real test sites are assumed to be flat. A flight planning exercise is performed with both sensors with a maximum 40 deg FOV. Data density is allowed to vary in a range of 1.5 to 2.0 $\mathrm{points/m^2}$ that amounts to a 33% variation in data density. Further, as stated earlier, a maximum of 10% variation in across-track and along-track spacings are adopted for each site. Considering the potential of the demonstrated GA-based automatic flight planning process which does not require any human

Fig. 8 Big Smith Creek site in Mackenzie valley of Canada.

Fig. 9 Harry Channel site in Mackenzie valley of Canada.

intervention for decision making, the authors preferred to perform 30 runs for each site, and the best results along with the values of the FD are reported below.

With the results (as shown in Tables 6 and 7) obtained by the GA-based flight planning system for the BSC AOI and HC AOI, the following salient observations are drawn:

1. As the BSC and HC sites are, respectively, close to a rectangular and square shape, the desired flying direction is obviously known (i.e., along the longer side of the rectangle or square). Flying directions for the BSC site with two sensors justify it as both values are approximately 270 deg (as shown in Table 6). However, for the HC site (as shown in Table 7), which is close to square in shape, flying is possible along either the longer or shorter edge of the AOI. While working with the ALTM 3100EA sensor, the flying direction is determined by the flight planning system along the longer edge (∼145 deg). Conversely, with the ALS50-II sensor, the flying direction is determined along the shorter edge (∼230 deg).
2. The values of data densities, which may be calculated by the flight planning parameters tabulated in Tables 6 and 7 for the BSC and HC sites, are in the range of 1.5 to 2.0 points/m^2. However, for both sites, while working with the ALTM 3100EA sensor, calculated values of the data densities are close to 1.5 points/m^2. On the contrary, with the ALS50-II, calculated values of data densities for both sites are close to 2.0points/m^2.

Table 6 Flight planning parameters and flight duration for Big Smith Creek AOI.

	Values	
Parameter	ALTM 3100EA	ALS50-II
Flying height (H)	1428.747 m	1106.179 m
Flying direction (θ)	269.128 deg	269.995 deg
Aircraft speed (V)	45.60 m/s	53.05 m/s
Scanning frequency (f)	30 Hz	32.6 Hz
Half scan angle ($\pm\phi$) or FOV (2ϕ)	± 19 deg	40 deg FOV
PRF (F)	70 kHz	81,300 Hz
Flight duration (T)	514.1 s	497.5 s

Table 7 Flight planning parameters and flight duration for Harry Channel AOI.

	Values	
Parameter	ALTM 3100EA	ALS50-II
Flying height (H)	1566.632 m	1183.335 m
Flying direction (θ)	145.395 deg	230.747 deg
Aircraft speed (V)	45.48 m/s	47.63 m/s
Scanning frequency (f)	29 Hz	30.5 Hz
Half scan angle ($\pm\phi$) or FOV (2ϕ)	± 18 deg	40 deg FOV
PRF (F)	70 kHz	76,000 Hz
Flight duration (T)	1748.6 s	1677.2 s

This proves that under the given requirements of data for the BSC and HC sites, the ALS50-II sensor will capture denser data compared to the ALTM 3100EA sensor.

3. The FD with the ALS50-II sensor is less than that provided by the ALTM 3100EA sensor for both BSC and HC sites.

The above observations can be explained by analyzing the characteristic features of the two sensors with the given requirements and the two AOIs. These observations are predominately because of different combinations of flight planning parameters available with the two sensors. Due to fewer options for the PRF and a higher value of least counts for other parameters with the ALTM 3100EA sensor, numbers of combinations of the parameters are less when compared against the possible combinations of the ALS50-II sensor. This is the primary reason that although the flight planning system determines the flying direction along the shorter edge for the HC AOI, the FD is less with the ALS50-II sensor. Further, larger numbers of combinations provide more flexibility in decision making by the GA with the ALS50-II sensor. Therefore, working with the ALS50-II sensor for the BSC or HC test sites is more economical.

6 Conclusion and Future Work

The authors propose a new methodology for flight planning, which automatically determines the flight planning parameters without any initial estimate for airborne LiDAR by minimizing the FD using a GA. The proposed approach derives the FD and sensor parameters. Unlike conventional approaches, the FD is modeled as consisting of the ST and TT. The user requirements, scanner hardware limitations, and the mapping standards are accounted for by deriving formulations to represent these as constraints with the objective function (FD). Considering that the constraints and FD are discontinuous mathematical functions of the nonseparable continuous flying parameters and discrete scanner parameters, the RGA code is employed for optimization. Moreover, the proposed method of constrained minimization of the FD is performed with two distinct and commercially available LiDAR sensors.

In order to test the performance of the GA, intuitively obvious cases of airborne LiDAR data acquisition over a long strip and triangular AOI are attempted. The RGA code successfully derives the flight planning parameters automatically, including the intuitive flying direction for both cases. In addition to this, the authors have shown the pitfalls of either ignoring the TT or assuming it as a constant by presenting results for an intuitively obvious long rectangular AOI. Similarly, using an intuitively obvious triangular AOI, the authors have also shown the effect of ignoring the cushion period, which may lead to an incorrect flight plan causing a longer flight duration and, thus, higher cost. As a result, this proves that the hypothesis of constant or zero TT is inferior to selecting an appropriate model of the TT.

For an arbitrarily chosen AOI, the flight planning by the GA reveals that increasing the population of the GA improves the consistency due to an exhaustive and rigorous search and, thus, provides higher confidence, efficiency, and accuracy for hitting the optimum solution. After removal of the outliers, the statistical results of the flight planning parameters are obtained. In order to validate the correctness of the results (values of flight planning parameters) for the simulated AOI for the chosen LiDAR sensors, artificial LiDAR data are generated using a LIMULATOR utility. The standard test recommended by Heidemann[16] for the NPS is satisfied by the data sets, which are generated by flight planning parameters determined for both sensors. Thus, the authors prove the statistical validity, which establishes the feasibility and acceptance of the proposed approach.

The approach developed for a GA-based automatic flight planning system is implemented for two real test sites with two sensors. Analysis of the observations on the obtained flight planning parameters is presented for establishing the relative comparison of the performances of the two sensors for two sites. The comparison also emphasizes the economic aspects of the sensor selection for the two sites.

Finally, in this study, it is realized that compared to the conventional time-consuming approach of flight planning, the presented approach requires a computational time that can be predicted in advance. Moreover, the flexibility and versatility of the presented approach simultaneously accommodates all types of continuous and discrete variables with any number of constraints in the FD minimization problem. Therefore, in the future, the proposed approach can be developed in a more comprehensive manner to include all the possibilities of flight planning, such as wind speed, variation of data density and overlap with terrain elevation, simultaneous photographic data acquisition, TT for nonconsecutive turning mechanisms, field limitations, and preferences of the flying crew. Further, configurations of the GA for minimum outliers should be developed. In addition to that, experimental validation in real terrains using all types of sensors mounted in aerial vehicle should also be performed as a benchmarking exercise for the proposed approach of flight planning.

References

1. J. W. van der Vegt and A. Hoffmann, "LiDAR hits the spot—airborne laser scanning reaches maturity," *Geoinformatics*, 32–39 (2001).
2. W. Uddin, "Evaluation of airborne LiDAR digital terrain mapping for highway corridor planning and design," in *Proc. Pecora 15/Land Satellite Information IV/ISPRS Commission I/FIEOS 2002 Conf.*, 2002, http://www.isprs.org/proceedings/XXXIV/part1/paper/00027.pdf (13 July 2014).
3. D. Gatziolis and H. Anderson, "A guide to LiDAR data acquisition and processing for forests of the Pacific Northwest," General Technical Report PNW-GTR-768, United States Department of Agriculture, Forest Service, Pacific Northwest Research Station (2002).
4. TRB, "Research results digest 10: light detection and ranging (LiDAR) deployment for airport obstruction surveys," 2010, http://www.trb.org/Main/Blurbs/163789.aspx (20 January 2014).
5. K. Saylam, "Quality assurance of LiDAR systems—mission planning," in *ASPRS 2009 Annual Conf., American Society for Photogrammetry and Remote Sensing*, Baltimore, Maryland, American Society for Photogrammetry and Remote Sensing, USA (2009).
6. N. C. May, "A rigorous approach to comprehensive performance analysis of state-of-the-art airborne mobile mapping systems," PhD Thesis, The Ohio State University, Ohio (2008).
7. E. Walker, "A slide rule for the computation of precision turns in air survey navigation (the I.T.C. survey flight slide rule)," *Photogramm. Rec.* **4**(24), 489–502 (1964).
8. A. Dashora and B. Lohani, "Turning mechanisms for airborne LiDAR and photographic data acquisition," *J. Appl. Remote Sens.* **7**(1), 073488 (2013).
9. A. Combrink, E-mail communications with Dr. Adriaan Combrink, C K Aerial Surveys, South Africa, private communications (25 August 2011 to 11 October 2012).
10. X. Tian et al., "Design on the aerial survey parameters of the airborne LiDAR," in *2011 Int. Conf. on Remote Sensing, Environment and Transportation Engineering*, Nanjing, China, pp. 214–217, IEEE, USA (2011).
11. A. Dashora, B. Lohani, and K. Deb, "Two-step procedure of optimisation for flight planning for airborne LiDAR data acquisition," *Int. J. Math. Model. Numer. Optim.* **4**(4), 323–350 (2013).

12. E. P. Baltsavias, "Airborne laser scanning: basic relations and formulas," *ISPRS J. Photogramm. Remote Sens.* **54**, 199–214 (1999).
13. A. Wehr and U. Lohr, "Airborne laser scanning—an introduction and overview," *ISPRS J. Photogramm. Remote Sens.* **54**, 68–82 (1999).
14. WSI., "Minimum LiDAR data density considerations for the pacific northwest," 2010, http://www.oregongeology.org/sub/projects/olc/minimum-lidar-data-density.pdf (20 January 2014).
15. A. Combrink, "An introduction to LiDAR-based aerial survey (part 2)," 2011, http://www.ee.co.za/wp-content/uploads/legacy/posit11/posit-jun11-p20-24.pdf (30 June 2014).
16. H. K. Heidemann, "LiDAR base specifications (version-1)," 2012, http://pubs.usgs.gov/tm/11b4/ (20 January 2014).
17. A. Dashora, "Optimization system for flight planning for airborne LiDAR data acquisition," Ph.D. Thesis, Dept. of Civil Engineering, Indian Institute of Technology Kanpur, Kanpur, India (2013).
18. K. Kraus, "Appendices," in *Photogrammetry*, pp. 432–435, Walter De Gruyter, Berlin, Germany (2004).
19. J. S. Wolper, "Turn performance of aircraft," *SIAM Rev.* **36**(3), 470–473 (1994).
20. Optech, *ALTM 3100EA Enhanced Accuracy*, Optech Inc., Canada (2008).
21. Leica, *Leica's ALS50-II Airborne Laser Scanners Product Specifications*, Leica Geosystems, Switzerland (2007).
22. M. Boba, Optech, *ALTM 3100EA Enhanced Accuracy*, Optech Inc., Canada (2008).
23. J. Carroll, Bearing Tree Land Surveying L.L.C., USA (20 February 2009).
24. D. E. Goldberg, "A gentle introduction to genetic algorithms," in *Genetic Algorithms in Search, Optimization, and Machine Learning*, pp. 1–25, Pearson Education Asia, Delhi (1989).
25. DGCA., "Establishments of minimum flight altitudes. Section 9—air space and air traffic management, civil aviation requirements," 8 January 2010, http://dgca.nic.in/cars/D9R-R1.pdf (20 January 2014).
26. B. Lohani, P. Reddy, and R. K. Mishra, "Airborne altimetric LiDAR simulator: an education tool," *Int. Arch. Photogramm., Remote Sens. Spat. Inf. Sci.* **36**(6), 179–183 (2006).
27. MERX, "Advance contract award notice—LiDAR acquisition at 8 stream crossing sites in the Mackenzie Valley—ACAN," 2011, http://www.merx.com/English/SUPPLIER_Menu.asp?WCE=Show&TAB=1&PORTAL=MERX&State=7&id=213336&print=Y&src=osr&ForceLID=&HID=&hcode=Abq36rzP95fNYP1b0PfZDw%3D%3D (7 May 2014).

Ajay Dashora received his MTech and PhD degree in geoinformatics specialization from the Department of Civil Engineering, Indian Institute of Technology Kanpur, India, in 2005 and 2013, respectively. He is currently an assistant professor at the Institute of Infrastructure, Technology, Research and Management (IITRAM), Ahmedabad, India. His research interests include physical modeling, synthetic simulation, compatibility studies, integration of airborne data acquisition methods and techniques, use of evolutionary algorithms in remote sensing, and application of remote sensing techniques in natural resource exploration and management.

Bharat Lohani received the PhD degree from the University of Reading, Reading, United Kingdom, in LiDAR technology and environmental sciences, in 1999. He is currently a professor with the Indian Institute of Technology Kanpur, Kanpur, India, where he has been since 2002. He has interest in teaching and research in the domain of laser scanning-data capture, processing and application development. He is currently co-chair with ISPRS WG V-2 and a fellow with the Institution of Surveyors, India.

Kalyanmoy Deb is endowed chair professor of electrical and computer engineering at Michigan State University, USA. His research interests are in evolutionary optimization and their application in optimization, modeling, and machine learning. He was awarded the Infosys Prize, TWAS Prize in engineering sciences, Caj Astur Mamdani Prize, Distinguished Alumni Award from IIT Kharagpur, Edgeworth-Pareto award, and Bhatnagar Prize in Engineering Sciences. He is a fellow of IEEE and three science academies in India. He has published 350+ research papers with a Google scholar citation of 54,000+ with an h-index of 77. He is on the editorial board of 18 major international journals.